Extreme-ultraviolet Ramsey-type spectroscopy

Angela Pirri,[1] Emiliano Sali,[1,2] Chiara Corsi,[1] Marco Bellini,[1,3] Stefano Cavalieri,[1,2] and Roberto Eramo[1,2,4]

[1]*European Laboratory for Non-Linear Spectroscopy (LENS), Università di Firenze, Via N. Carrara 1, I-50019 Sesto Fiorentino, Firenze, Italy*

[2]*Dipartimento di Fisica, Università di Firenze, Via G. Sansone 1, I-50019 Sesto Fiorentino, Firenze, Italy*

[3]*Istituto Nazionale di Ottica Applicata (CNR), Largo E. Fermi 6, I-50125 Firenze, Italy*

[4]*INFM–CRS–Soft Matter (CNR), c/o Università la Sapienza Piazzale A. Moro 2, I-00185, Roma, Italy*

We performed an experimental and theoretical investigation of Ramsey-type spectroscopy in conjunction with high-order-harmonic generation. The ninth harmonic ($\lambda \simeq 88$ nm) of a femtosecond Ti:sapphire laser was used to excite a pair of autoionizing states of krypton. The outcome of the ionization process, detected by an ion-mass spectrometer, shows the characteristic quantum interference pattern. The behavior of the fringe contrast was interpreted on the basis of a simple analytical model, which reproduced well the experimental results without any free parameter.

PACS number(s): 32.80.Qk, 32.80.Zb, 32.80.Fb, 42.65.Ky

I. INTRODUCTION

In recent years there has been an increasing interest in high spectroscopic resolution in the vacuum ultraviolet and extreme ultraviolet (xuv) regions, where important investigations involving several atomic and molecular species can be performed [1–5]. A broad and simple tunability in all this spectral range and extending to the soft x rays is achieved only by synchrotron facilities, which, when used in combination with the best monochromators available, can provide radiation with a bandwidth as small as $0.5-1$ cm^{-1} [6]. Apart from their limitations in spectral resolution, synchrotron sources suffer from not being user friendly: indeed, table-top-size sources would be much more desirable for a more widespread use. On the other hand, laser-based narrowband cw sources hardly exist at such short wavelengths [7].

Recent developments in this field of research have been triggered by the increasing availability of new generations of pulsed laser sources. These pulsed lasers permit one to reach very high peak intensities and consequently to induce nonlinear processes of extremely high order. In this way, very short wavelengths can be generated using table-top setups [8,9]. These sources mainly fall into two categories: those based on the frequency up-conversion of nanosecond pulses using low-order nonlinear processes, such as four- and six-wave mixing, and those relying on high-order-harmonic generation using laser pulses of femtosecond duration. The former approach has the advantage of an intrinsically narrow bandwidth which can be directly used for high-resolution spectroscopic studies: however, the short-wavelength extension of these resonant nonlinear techniques is limited to about 20 eV [10]. The latter approach, based on ultrashort laser pulses interacting in a nonresonant way with noble gas atoms, has the capability to extend the generated spectrum much further into the xuv and soft x-ray regions but it is inherently affected by a broad bandwidth, which has so far limited its use mainly to time-resolved studies. An "intermediate" approach compared to these two has also been employed, based on the use of pump laser pulses of intermediate duration (a few hundred picoseconds) in order to generate

medium-order harmonics in a trade-off between spectral resolution and spectral extension [11].

However, the situation has been rapidly evolving in recent years and several experiments have shown that it is possible to obtain a high-spectral resolution without losing the advantages of using high-order harmonics generated by ultrashort laser pulses. These novel approaches hold the potential to extend the realm of high-precision spectroscopic studies to unexplored spectral regions and to give access to a wealth of new data. The general idea that lies at the basis of all these new schemes is similar to what was first introduced by Ramsey in 1950 [12] to deal with the transit-time-limited interaction between the molecules in a jet and a microwave field. In that case a greater effective interaction time was obtained by using two widely spaced interaction zones. In an analogous way one may think to extend the interrogation time characteristic of an ultrashort harmonic field by using pairs (or sequences) of collinear, phase-coherent, and time-delayed pulses [13–16]. In a very simple representation of this idea, a first short pulse may be thought of as inducing a coherence in a two-level system, creating a dynamical polarization of the medium. The induced polarization then oscillates at the transition frequency with an amplitude that decays on the time scale of its characteristic dephasing time. Depending on the phase delay of the second pulse, this may either further excite the system or bring it back to the ground state. As a result, any excitation-related observable exhibits interference fringes when the delay between the two pulses is varied. Important spectroscopic information such as the absolute frequency of the transition, the dephasing time, or the energy separation of nearby states can be extracted with this method.

The extension of this technique to high-order harmonics in the xuv is not straightforward. Obtaining a pair of phase-locked and time-delayed harmonic pulses is made difficult by the lack of suitable optics in the xuv region, where a Michelson interferometer cannot be built. A solution to this problem was found by transferring the pulse splitting and delay from the harmonic to the pump beam, and relying on the phase coherence of the generation process [17,18]. Experiments were performed in order to check the possibility of

producing a phase-locked pulse pair from two phase-locked collinear pump pulses: the results of optical tests suggested that this is indeed possible, at least in a delimited intensity range [19,20]. The use of such a *Ramsey-type* excitation was suggested as a spectroscopic tool for states embedded in the continuum, i.e., autoionizing states, even when the continuum part of these states plays a relevant role in the dynamics of the system [3].

The first experimental demonstration of Ramsey-type spectroscopy with high-order harmonics was presented by our group a few years ago [4]. In that experiment a couple of autoionizing states of krypton were excited by a pair of pulses at $\lambda \simeq 88$ nm, the ninth harmonic of a Ti:sapphire laser. The observation of quantum interferences in the ionization signal allowed us to extract useful spectroscopic information. A slightly different scheme, relying on the analysis of interferograms to recover the harmonic spectra, demonstrated the feasibility of an xuv extension of the Fourier-transform spectroscopy technique, but has not been applied to any atomic or molecular study so far [5]. More recently, important results along the lines of the two-pulse Ramsey excitation scheme have been obtained for the spectroscopy of a bound state at 125 nm in xenon and for a two-photon transition at 212 nm in krypton [1,2]. In these experiments the pump pulse pair was obtained by amplifying a pair of successive pulses of the oscillator train and their delay was set with an unprecedented accuracy by controlling the repetition rate of the phase-stabilized femtosecond mode-locked laser. However, the ultimate frontier in xuv high-resolution spectroscopy will possibly involve the use of long, phase-locked, trains of pulses instead of simple pairs, in order to obtain a comb of narrow spectral modes. The first experiments have already proved the possibility of obtaining such a train of xuv pulses by producing harmonics at a high repetition rate in a femtosecond enhancement cavity [21–23]. The development of this technique will probably allow the frequency comb advantage in terms of extremely precise frequency measurements to be extended to the xuv. Although these recent techniques have the potential to go much beyond the current resolution limits in the xuv range, the original Ramsey scheme demonstrated in [4] may still prove extremely useful in order to perform high-resolution spectroscopy with a relatively simple experimental setup which does not require complex phase-stabilized lasers.

In this paper we present an extension of our previous study of Ramsey-type spectroscopy [4] using the same combination of laser frequency and atomic levels. Compared to our previous work, in this study several changes were introduced in order to make the experimental results and their comparison with theory more robust. In addition to a general improvement of the experimental setup, which allowed us to perform the experiments exploiting the full repetition rate of our laser, the most important change is the choice of collecting ions instead of electrons, which allows a comparison between theory and experiment free of unknown parameters. Also, for the theoretical model, an analytical solution was found that is able to reproduce satisfactorily the experimental data with no unknown parameters.

The structure of the paper is the following. In Sec. II we present the theory at the basis of the experiments and the
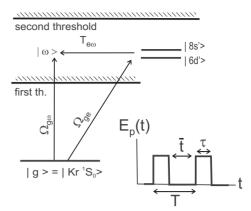

FIG. 1. Scheme of the interaction, showing the involved autoionizing levels of the krypton atom. Ω_{ge} is the Rabi frequency for the coupling between the ground state $|g\rangle$ and each autoionizing state $|e\rangle$; as explained in the text, we are working in a perturbative regime and a simple two-state dynamics involving the ground state and a single autoionizing state has to be taken into account. $\Omega_{g\omega}$ is the analog for the continuum states $|\omega\rangle$. The coupling between the autoionizing state and the continuum, due to an intra-atomic interaction, has been denoted by $T_{e\omega}$. Bottom right: temporal scheme of the pulse pair as treated in the theory, i.e., flat top, duration τ, delay T, separation $\bar{t} = T - \tau$.

calculations, namely, the two-state theory, with some analytical results and the calculation performed in the actual case for the comparison with the experimental data. In Sec. III we describe the experimental setup, with particular emphasis on the main changes introduced in this work with respect to our previous one. In Sec. IV we present the experimental results and the comparison with theoretical calculations. Finally, in Sec. V a brief summary is presented.

II. THEORY

In a two-state approach, the atomic system ground state $|g\rangle$ is coupled to the autoionizing state $|e\rangle$ by means of a field at frequency ω_p (see Fig. 1). We start from the atomic state vector expansion

$$|\Psi\rangle = c_g(t)|g\rangle + c_e(t)|e\rangle + \int d\omega \, c_\omega |\omega\rangle \qquad (1)$$

in terms of the bound and continuum states. We work in the interaction picture, and use the rotating wave approximation and the usual procedures of Markov elimination for the continuum amplitude to get

$$\left(\frac{d}{dt} + \frac{\Gamma_g}{2}\right) c_g = \frac{i\gamma}{2}(-q + i) e^{i\Delta t} c_e, \qquad (2)$$

$$\left(\frac{d}{dt} + \frac{\Gamma_e}{2}\right) c_e = \frac{i\gamma}{2}(-q + i) e^{-i\Delta t} c_g. \qquad (3)$$

In these equations, the notations

$$\Gamma_g = \left(\pi \frac{\Omega_{g\omega}\Omega_{\omega g}}{2}\right)_{\omega=\omega_0}, \quad \Gamma_e = 2\pi[T_{e\omega}T_{\omega e}]_{\omega=\omega_0},$$

$$\gamma = \pi(\Omega_{g\omega}T_{\omega e})_{\omega=\omega_0} = \sqrt{\Gamma_g\Gamma_e},$$

$$q = \frac{\int d\omega \Omega_{g\omega}T_{\omega e}/(\omega - \omega_0) + \Omega_{ge}}{\pi(\Omega_{g\omega}T_{\omega e})_{\omega=\omega_0}}, \quad \Delta = \omega_g + \omega_p - \omega_e$$

have been used for the decay constants Γ_g and Γ_e, the coupling constant γ, the Fano parameter q, and the detuning Δ. In these definitions $\omega_0 = \omega_g + \omega_p \approx \omega_e$ is the frequency in the continuum where the laser is tuned, $\Omega_{\omega k} = E_p\langle\omega|\mathbf{d}\cdot\hat{\mathbf{e}}|k\rangle/\hbar$ $(k=g,e)$ are the Rabi frequencies,

$$\mathbf{E} = E_p\hat{\mathbf{e}}\cos\omega_p t$$

is the (linearly polarized) probe field, and $T_{\omega k}$ are the matrix elements of the autoionizing interaction. In (2) and (3), the dynamic and static Stark shifts $\delta\omega_g$ and $\delta\omega_e$ are thought of as included in the detuning.

An explicit analytical result for the ionization probability I can be obtained assuming two identical pulses of duration τ and delay T, with $T \geq \tau$ (see Fig. 1, bottom right), and a resonant interaction, i.e., $\Delta\tau \approx 0$. Following Ref. [3] one can obtain $c_g^{(k)}$ and $c_e^{(k)}$, i.e., the parts of the amplitudes which are of the order of the Rabi frequency $(\Omega_{g\omega})^k$. In this way, the ionization probability $I = 1 - |c_g(T+\tau)|^2$ is given by

$$I = 2I_1 + (q^2+1)I_f e^{-\Gamma_e(T-\tau)/2}\cos(\nu + \omega_{eg}T) \qquad (4)$$

where

$$\tan\nu = \frac{2q}{q^2-1}, \qquad (5)$$

$$I_f = \frac{1}{2}\int_0^\tau dt'' \gamma(t'') e^{-\Gamma_e(\tau-t'')/2}\int_0^\tau dt' \gamma(t') e^{-\Gamma_e t'/2} \qquad (6)$$

and I_1 is the ionization probability characteristic of just one pulse:

$$I_1 = 1 - |c_g(\tau)|^2 = \int_0^\tau dt'\Gamma_g(t') + \frac{q^2-1}{2}\int_0^\tau dt'\gamma(t')$$
$$\times \int_0^{t'} dt''\gamma(t'')e^{-\Gamma_e(t'-t'')/2}. \qquad (7)$$

In the limit $T\to\infty$, we recognize from Eq. (5) the ionization probability of the single pulse multiplied by 2.

If we now assume flat-top pulses (as in Fig. 1, bottom right) the expressions (6) and (7) assume the following explicit forms:

$$I_f = \frac{2\Gamma_g}{\Gamma_e}(1 - e^{-\Gamma_e\tau/2})^2, \qquad (8)$$

$$I_1 = \Gamma_g\tau + (q^2-1)\Gamma_g\left(\tau + \frac{2}{\Gamma_e}(e^{-\Gamma_e\tau/2} - 1)\right). \qquad (9)$$

We can now define the following two quantities, i.e., the maxima and minima of the ionization yield I as a function of the separation $\bar{t} = T - \tau$ between the two pulses:

$$I_\pm = 2I_1 \pm (q^2+1)I_f e^{-\Gamma_e\bar{t}/2}, \qquad (10)$$

and from these we can write the fringe contrast as

$$\rho = \frac{I_+ - I_-}{I_+ + I_-} = \frac{(q^2+1)(1 - e^{-\Gamma_e\tau/2})^2 e^{-\Gamma_e\bar{t}/2}}{\Gamma_e\tau + (q^2-1)\Gamma_e[\tau + (2/\Gamma_e)(e^{-\Gamma_e\tau/2} - 1)]}. \qquad (11)$$

The previous expression, although limited to one state only and resonant excitation, already gives some insight into the physics underpinning the process. In particular, if we assume $\Gamma_e\tau \ll 1$ (i.e., pulse duration much shorter than the lifetime of the autoionizing state), expression (11) becomes

$$\rho \simeq \frac{(q^2+1)\Gamma_e\tau e^{-\Gamma_e\bar{t}/2}}{4 + \Gamma_e\tau(q^2-1)}. \qquad (12)$$

We note that in the limit $q\to\infty$ we find $\rho \sim e^{-\Gamma_e\bar{t}/2}$, i.e., the typical behavior of a bound state, which is obtained when the upper state population is measured [13]. On the other hand, for q "moderate" (e.g., $q \simeq 2$), then $\rho \sim q^2\Gamma_e\tau e^{-\Gamma_e\bar{t}/2}$. For $\tau\to 0$ we get $\rho\to 0$, which is a completely different behavior from the case of a bound state.

Expression (11) was obtained for one autoionizing state only and assuming resonant excitation (detuning $\Delta=0$). In order to have a theoretical quantity that can provide a meaningful comparison with our experimental data, it is necessary for our model to include a detuning $\Delta\neq 0$ and the presence of a second autoionizing state. The introduction of the detuning leads to the following expression for the ionization yield:

$$I = 2\,\mathrm{Re}\left\{\Gamma_g\left[\tau + \frac{\Gamma_e}{2}(i-q)^2 \times \left(\frac{\tau}{\Gamma_e/2 - i\Delta} + \frac{e^{(-\Gamma_e/2 + i\Delta)\tau} - 1}{(\Gamma_e/2 - i\Delta)^2}\right)\right.\right.$$
$$+ \frac{\Gamma_e}{4(\Gamma_e/2 - i\Delta)^2}(i-q)^2 e^{-i\omega_{eg}T}e^{-\Gamma_e\bar{t}/2}e^{-i\Delta\tau}$$
$$\left.\left.\times(1 - e^{(-\Gamma_e/2 + i\Delta)\tau})^2\right]\right\}. \qquad (13)$$

As long as we work in the perturbative regime, no coupling exists between the two autoionizing states, which thus evolve independently following a two-state dynamic. In our experiment, as schematically shown in Fig. 1, the two excited autoionizing states of krypton that we are interested in are $4p^5(^2P_{1/2})6d'$ and $4p^5(^2P1/2)8s'$. They have an energy separation of about 29 meV, well below the 0.21 eV of the single-pulse spectral width. Both of them are thus simultaneously excited by the ninth harmonic of our laser at 88.2 nm. The theoretical ionization probability including both states is then simply obtained by summing up the independent contributions of two single states with proper choice of the values of energy and detuning. As a consequence of the difference in energy between the two states, a beating should be visible in a plot of the fringe contrast of the ionization signal as a function of the delay between the pulses. In the present situation, where the lifetimes of the two states are of a different order of magnitude (461 fs for the $8s'$ and 26 fs for the $6d'$) the "delay window" where the beating is observable is determined by the equality between the ion modulations of the two states. The period of the beating is
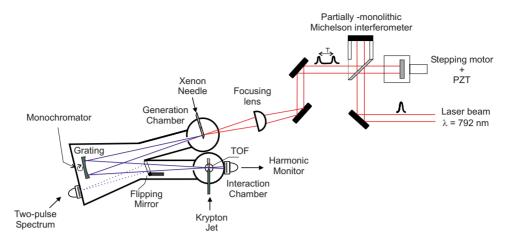
FIG. 2. (Color online) Experimental setup. The ninth harmonic, generated by focusing the phase-locked laser pulse pair produced by the Michelson interferometer in the xenon flow and selected by the xuv monochromator, is focused in the krypton jet in the interaction chamber. The ions ejected in the one-photon ionization process are energy analyzed by a time-of-flight (TOF) spectrometer. A flipping mirror can redirect the harmonic field to the exit slit of the monochromator, where a spectrum of the two-pulse field can be measured and used for the fine alignment of the Michelson interferometer. A phosphor-phototube pair, at the exit of the interaction chamber, monitors the transmitted harmonic field intensity.

determined by the difference in the energy of the two states. Indeed, a beating is clearly visible in the curves of Figs. 5 and 6.

To summarize, in our analytical model we assume the harmonic field to be made of a pair of flat-top pulses, with a full width at half maximum duration of 17 fs derived from the measured 1.4 nm linewidth of the single-pulse harmonic spectrum. The parameters that we introduce in the model, i.e., the state energy, energy widths, ionization constants, and Fano parameters, are those reported in the synchrotron measurement of Ref. [24]. In our experiment we chose to measure the ion signal instead of electrons, which implies that no parameter remains unknown. This allows a more strict comparison with the experimental results, as will be extensively discussed in the next sections.

III. EXPERIMENTAL APPARATUS

The experimental apparatus, schematically shown in Fig. 2, is composed basically of four units (plus the laser system): the Michelson interferometer, the harmonic generation chamber, the xuv monochromator, and the interaction chamber. Each of these stages presents some improvements or changes with respect to the previous work.

The light source is an amplified Ti:sapphire laser delivering pulses with up to ~1 mJ energy per pulse, ~30 fs time duration at a repetition rate of 1 kHz, with central wavelength set at 793.7 nm. The laser pulse passes through a Michelson interferometer, which divides the fundamental pulse into two replicas by means of a 50:50 beam splitter. The relative delay between the two pulse replicas can be varied by translating the folding mirror in one arm of the interferometer. Long translations are obtained using a computer-controlled stepping motor, while shorter scans are obtained by applying a triangular-wave voltage to a piezoelectric crystal that holds the mirror.

Great attention was devoted to reducing as much as possible any possible source of mechanical instabilities in order

to increase the accuracy of the measurement. A partially-monolithic quartz interferometer was chosen and the whole device was covered by a Plexiglas box and isolated from the optical table by means of antivibration plastic sheets. Mechanical and thermal drifts around 10–20 nm/min were experimentally estimated.

The laser beam is focused in the first vacuum chamber by a 25-cm-focal-length plane-convex lens. An intensity of about 5×10^{14} W/cm^2 is reached in the focal spot, where a steel capillary containing xenon is placed. The laser itself drills two holes in the capillary (entrance and exit) with a diameter of approximately 50 μm each. The gas flows continuously through these holes, allowing for a temporally constant xenon pressure profile in the spot where harmonics are generated.

The generated harmonic radiation enters the xuv monochromator, where it is spectrally separated and refocused by a Pt-Ir normal-incidence spherical grating (600 lines/mm), which selects for our purpose the ninth harmonic, corresponding to a wavelength of 88.2 nm. The refocused harmonic then interacts with the krypton atoms inside an ion-mass time-of-flight (TOF) spectrometer, which replaces the exit slit of the monochromator (more details about the interaction region are provided towards the end of this section).

The TOF spectrometer is equipped with three molybdenum disks where dc extraction fields up to 250 V/cm are applied for efficient charge collection. The interaction region is placed between the first two plates, where a continuous flow of krypton atoms is injected by means of a needle, perpendicularly to the TOF axis and to the harmonic field propagation. The charges leave the interaction volume through a 2-mm-diameter aperture on the second and third molybdenum plates, and enter a field-free zone. The flight tube is a 35-cm-long, gold-plated, copper cylinder with a diameter of 5 cm. In order to prevent external magnetic field effects, a coaxial μ-metal cylinder encloses both the flight tube and the interaction region. A microchannel plate assembly placed at the end of the field-free zone detects the ions.

The time-resolved signal is amplified and shaped by a fast constant fraction discriminator and sent to a fast multiscaler PC board with ~0.5 ns time resolution. Finally it is stored in a computer and analyzed.

A very critical element for the experiment is the collinear alignment of the two harmonic beams. With this aim, a first check is done on the alignment of the two infrared beams coming out of the interferometer, by visually inspecting (using an infrared-sensitive card) the optical interference fringes that they produce. Fine alignment is performed by means of three piezoelectric crystals acting on the kinematic mounts of the folding mirror in one arm of the interferometer. During the measurements a similar check is kept "online" using a He-Ne laser beam that enters the interferometer collinearly with the infrared laser and checking the fringes on the He-Ne profile. This check allows us to control the alignment of the two infrared pulses by monitoring pulse front displacements of the order of hundreds of nanometers over the beam diameter. Once the two infrared beams are aligned to the best of our capabilities, a second, more stringent alignment check is done directly on the harmonic beams. In fact, after being separated by the grating, the harmonics can be either directed into the interaction chamber, or deviated by a flipping mirror towards an exit slit at the back of the monochromator (see Fig. 2), where they can be detected by means of a phosphor screen and a photomultiplier tube. By measuring the two-pulse spectrum and by maximizing the fringe contrast it is possible to optimize the horizontal alignment of the two harmonic beams on the scale of a fraction of the harmonic wavelength as shown in Ref. [20].

Let us now discuss the main experimental changes introduced in this work with respect to our previous study (Ref. [4]). These changes are essentially three: the different choice of detection configuration (ions instead of electrons), a different use of our xuv spectrometer as a harmonic selector, and the full exploitation of the kilohertz repetition rate of the laser system.

Concerning the choice of the charge detection configuration, in this study we decided to detect ions as a product of the ionization, and we aimed at confirming the results obtained in the previous work with an electron-detection configuration. At that time, the main reason for that choice was essentially that in principle the electron spectra could provide a more stringent monitor over the resonance condition. As a matter of fact, in the end this request did not turn out to be essential in the analysis of the results. On the other hand, the choice of detecting electrons implied that a parameter to be considered was the branching ratio between the differential ionization cross-sections of the $8s'$ and $6d'$ states along the direction of detection. This parameter is not known from the literature; therefore, in the fit of experimental data in Ref. [4], it was left as a free parameter. In contrast, this parameter does not exist if one detects ions instead of electrons, since the higher mass of ions implies that effectively they can be considered as motionless immediately after ionization. For this reason, the comparison of experimental and theoretical results that is presented in this study represents a much more stringent test, since no unknown parameter is left free.

As far as the second improvement is concerned, it is necessary to examine the optical properties of the xuv spectrom-
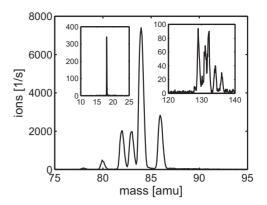

FIG. 3. Typical ion-mass spectrum. In addition to the krypton ions, the spectrum shows the presence of water (top left inset) and xenon (top right inset) coming from the harmonic generation chamber.

eter used to select and focus the ionizing harmonics. Due to the intrinsic astigmatism of its spherical grating, the monochromator, when used as a reflective optic (zero order), generates two foci that are two nearly linear images of the harmonics generating spot. The primary image is a line parallel to the slit direction and to the ion spectrometer axis (vertical) and should be used to optimize the spectral resolution of the monochromator itself. This focus is the "ordinary" focus for the xuv monochromator, as it represents the position where maximal spectral resolution (in the horizontal direction) is obtained. However, this position is not the ideal one as far as the resolution of the ion-mass spectrometer is concerned, since its axis is in the vertical direction. The secondary focus is separated by the primary one by about 2.5 cm and it appears as a horizontal line, 3.0 mm long and 30 μm wide (measurements performed using a charge-coupled device camera at zero order of the third harmonic). In order to enhance the resolution of the TOF spectrometer, whose axis is in the vertical direction, this is indeed the correct position as regards the focusing of the ionizing harmonic radiation, and therefore this position was chosen in this work as the point of interaction between the harmonic radiation and the krypton atoms. It should also be noted that the horizontal length of the focal image at this position is about ten times longer than the linear dispersion of the ninth harmonic. This means that all the spectral discrimination is completely lost at this position. This characteristic is an important issue as far as an easy comparison of the experimental results with the theory is concerned.

In Fig. 3 a typical ion spectrum is presented. It can be seen that the different isotopes are clearly resolved in the spectrum, implying a mass resolution better than 1 amu. This is due to the fact that, choosing the secondary focus of the spectrometer, the dimension of the beam along the TOF axis is so small (30 μm) that we keep the advantage of a two-dimensional collecting geometry. The choice of the primary focus would not have allowed this level of mass resolution, as the dimension of the beam along the time-of-flight spectrometer axis would have been too large. As a drawback, the 3 mm size in the horizontal direction implies a slightly reduced collection efficiency, since particle collection of our TOF spectrometer is only efficient over an area of diameter
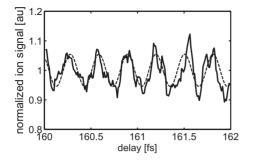
FIG. 4. Detail of the fringe pattern in the normalized ion signal (continuous curve) around a delay $\Delta t = 160$ fs. A sinusoidal fit (dashed curve) is superimposed. The fringe spacing corresponds to the 0.29 fs period of the atomic transition. Experimental points result from summing over 1200 laser pulses and smoothing on a fraction ($\approx 20\%$) of the fringe period.

of about 1 mm. On the other hand, this reduction of collection volume results in an advantage as far as the ease of wavefront superposition is concerned.

The last improvement with respect to our previous work is the full exploitation of the high (1 kHz) repetition rate of our Ti:sapphire laser. This was achieved by replacing the pulsed valves at 10 Hz with continuous-flow sources based on a metal capillary with holes. In this way we considerably increase the count rate of the experiment and thus reduce the time needed to obtain a measurement with sufficient stability and signal-to-noise ratio. We routinely worked with count rates of the order of 5000 ions/s, compared with the 10 electrons/s of the previous experiment.

IV. EXPERIMENTAL RESULTS AND DATA ANALYSIS

According to the theory (see Sec. II) the quantum evolution of the system reveals itself as a fringe pattern in the ion yield when the delay between the two harmonic pulses is varied. Figure 4 shows a typical fringe pattern measured around a delay $\Delta t \sim 160$ fs. During each measurement, all interesting signals are simultaneously acquired, i.e., the ion signal, the laser signals, and the transmitted harmonic intensity as a reference monitor. Each point of the continuous curve corresponds to the integrated signal of all ion peaks in the krypton spectrum, divided by the reference monitor. In the same figure a sinusoidal fit is superimposed to the experimental data, giving a measure of the fringe visibility. We notice the characteristic Ramsey modulation, with a period given by $2\pi/\omega_e \approx T_f/9 \simeq 0.29$ fs, T_f being the period of the fundamental laser beam.

The fringe contrast (open circles) versus the delay between the two xvu pulses is shown in Fig. 5. The solid curve is the theoretical calculation, obtained assuming flat-top pulses (see Sec. II). Precisely, the curve is obtained by summing up two contributions like expression (13) to take into account both states $8s'$ and $6d'$ of krypton. The agreement between the theoretical curve and the experimental data is quite good. The beating due to the energy difference between the two states, which is expected from the theory (continuous curve), can also be seen in the experimental results. As ex-
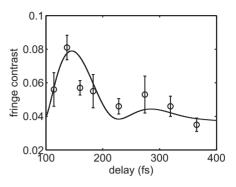

FIG. 5. Fringe contrast vs pulse delay. The solid curve superimposed to the data points is a theoretical curve, as explained in the text, where atomic parameters are obtained by the synchrotron radiation measurements of Ref. [24]. No free parameter has been used in the theoretical curve.

plained in Sec. II, the beating is observable only in a delay window where the ion modulations of the two states are comparable. This corresponds to a delay interval between 100 and 400 fs, i.e., intermediate between the lifetimes of the two states. As already mentioned earlier in the text, the theoretical curve is obtained without any free parameter (see Sec. II). In this respect, as far as the robustness of the comparison there is considerable difference between what is shown here in Fig. 5 and the similar figure in Ref. [4]: in that case one unknown parameter (the branching ratio between the differential ionization cross sections of the $8s'$ and $6d'$ states along the direction of detection) was left as a fit parameter, whereas here all parameters are known from the literature [24]. In order to stress the extent of the agreement between the experimental data and the model we also want to show how the theoretical curve is strongly dependent upon its parameters and how the agreement would be lost with different parameters from those that have been effectively measured and published. Figure 6 shows the results we would get by either increasing or decreasing by 20% only
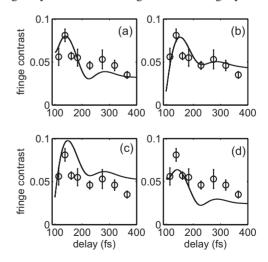

FIG. 6. Fringe contrast vs pulse delay, where the solid lines are theoretical curves (as in Fig. 5) obtained for varied values of the Fano parameter with respect to Ref. [24]. (a) q_{6d} increased by 20%, (b) q_{6d} decreased by 20%, (c) q_{8s} increased by 20%, and (d) q_{8s} decreased by 20%.

one parameter (namely, the Fano parameter q for either of the two states). It is clear to see that in these cases the agreement would be worse.

V. CONCLUSIONS

We showed that the time-delay spectroscopy (or Ramsey-type) technique, in conjunction with high-order-harmonic generation, is an efficient tool for high-resolution spectroscopic investigations in the xuv. The results of the experiment, performed on krypton atoms in resonance with a couple of autoionizing states, show a clear quantum interference in the ion signal and a beat between the doublet ion components. These quantum fringes are detected as a function of the delay between the two harmonic pulses.

These results confirm those that we obtained in a previous work on the same subject. As compared to that study, we introduced a few improvements to the experimental setup that made the results and their interpretation more robust. Most importantly, we chose a configuration of ion detection instead of electron detection. This choice allows us to theoretically model the process without any unknown parameter

left free, and the resulting model reproduces well the experimental data. The choice of ions also improved the statistics of our measurements, which also benefited from the full exploitation of the kilohertz repetition rate of the laser by replacing pulsed atom jets with continuous-flow sources.

We found that the main experimental limitation for a user-friendly spectroscopic application of this technique lies in the stability of the Michelson interferometer and in the wave front superposition of the two harmonic fields. We suggest that this last aspect can be overcome by detecting the signal from a smaller part of the volume of interaction between harmonic radiation and atomic samples.

[1] Stefan Witte, Roel Th. Zinkstok, Wim Ubachs, Wim Hogervorst, and Kjeld S. D. Eikema, Science **307**, 400 (2005).

[2] Roel Th. Zinkstok, Stefan Witte, Wim Ubachs, Wim Hogervorst, and Kjeld S. E. Eikema, Phys. Rev. A **73**, 061801(R) (2006).

[3] Stefano Cavalieri and Roberto Eramo, Phys. Rev. A **58**, R4263 (1998).

[4] Stefano Cavalieri, Roberto Eramo, Marzia Materazzi, Chiara Corsi, and Marco Bellini, Phys. Rev. Lett. **89**, 133002 (2002).

[5] M. Kovacev, S. V. Fomichev, E. Priori, Y. Mairesse, H. Merdji, P. Monchicourt, P. Breger, J. Norin, A. Persson, A. L'Huillier, C.-G. Wahlstrom, B. Carre, and P. Salières, Phys. Rev. Lett. **95**, 223903 (2005).

[6] P. A. Heinmann, M. Koike, C. W. Hsu, D. Blank, X. M. Yang, A. G. Suits, and Y. T. Lee, Rev. Sci. Instrum. **68**, 1945 (1997).

[7] K. S. E. Eikema, J. Walz, and T. W. Hansch, Phys. Rev. Lett. **86**, 5679 (2001).

[8] P. Salières, A. L'Huillier, P. Antoine, and M. Lewenstein, Adv. At., Mol., Opt. Phys. **41**, 83 (1999).

[9] Henry Kapteyn, Oren Cohen, Ivan Christov, and Margaret Murnane, Science **317**, 775 (2007).

[10] Th. A. Paul and F. Merkt, J. Phys. B **38**, 4145 (2005).

[11] F. Brandi, D. Neshev, and W. Ubachs, Phys. Rev. Lett. **91**, 163901 (2003).

[12] N. F. Ramsey, Phys. Rev. **78**, 695 (1950).

[13] M. M. Salour, Rev. Mod. Phys. **50**, 667 (1978).

[14] J. T. Fourkas, W. L. Wilson, G. Wackerle, A. D. Frost, and M.

D. Fayer, J. Opt. Soc. Am. B **6**, 1905 (1989).

[15] M. Bellini, A. Bartoli, and T. W. Hansch, Opt. Lett. **22**, 540 (1997).

[16] R. van Leeuwen, M. L. Bajema, and R. R. Jones, Phys. Rev. Lett. **82**, 2852 (1999).

[17] R. Zerne, C. Altucci, M. Bellini, M. B. Gaarde, T. W. Hänsch, A. L'Huillier, C. Lyngå, and C. G. Wahlström, Phys. Rev. Lett. **79**, 1006 (1997).

[18] M. Bellini, C. Lyngå, A. Tozzi, M. B. Gaarde, T. W. Hänsch, A. L'Huillier, and C. G. Wahlström, Phys. Rev. Lett. **81**, 297 (1998).

[19] P. Salières, L. Le Deroff, T. Auguste, P. Monot, P. d'Oliveira, D. Campo, J. F. Hergott, H. Merdji, and B. Carre, Phys. Rev. Lett. **83**, 5483 (1999).

[20] M. Bellini, S. Cavalieri, C. Corsi, and M. Materazzi, Opt. Lett. **26**, 1010 (2001).

[21] R. J. Jones, Kevin D. Moll, Michael J. Thorpe, and Jun Ye, Phys. Rev. Lett. **94**, 193201 (2005).

[22] C. Gohle, T. Udem, M. Herrmann, J. Rauschenberger, R. Holzwarth, H. A. Schuessler, F. Krausz, and T. W. Hänsch, Nature (London) **436**, 234 (2005).

[23] A. Ozawa, J. Rauschenberger, Ch. Gohle, M. Herrmann, D. R. Walker, V. Pervak, A. Fernandez, R. Graf, A. Apolonski, R. Holzwarth, F. Krausz, T. W. Hänsch, and Th. Udem, Phys. Rev. Lett. **100**, 253901 (2008).

[24] J. Z. Wu, S. B. Whitfield, C. D. Caldwell, M. O. Krause, P. van der Meulen, and A. Fahlman, Phys. Rev. A **42**, 1350 (1990).